IIT Madras

BTech Project

Diffuse interface method for condensation and evaporation on ideal and non-ideal surfaces

Aqel Ahammad K P
CH13B006

Guided by
Prof. Sumesh Thampi

May 9, 2017

Contents

1 Abstract **1**

2 Introduction **1**

3 Governing equations **2**

4 Lattice-Boltzmann method **2**

5 LB Method and Method of Lines **2**

6 Spinodal decomposition **3**

7 Surface tension **4**

8 Variation of phase field close to interfase **4**

9 Solid wall **5**

10 Evaporation of a planar droplet **5**

11 Condensation of planar droplet **6**

12 Evaporation and condensation of a sessile droplet on a solid surface **7**
12.1 Ideal surface 7
12.2 Hysteretic surface 8

13 Discussion and Conclusions **10**

14 Future work **10**

15 Source code **10**

Abstract

We model evaporation and condensation in this study using two methods - Lattice Boltzmann method and Method of lines. The two methods are evaluated based on space and time complexity, average time for one iteration and time for convergence. Evaporation of planar droplet is simulated and reproduced results recorded in the literature. Reversing the boundary condition for evaporation, we observe condensation. We study evaporation and condensation of a sessile droplet on ideal and hysteritic surfaces. The results show same pattern that is recorded experimentally. Pinning of contact line during evaporation is achieved on a hysteretic surface by defining a smaller receding angle.

Introduction

Recent developments in computational fluid dynamics have inspired researchers to simulate evaporation and condensation on surfaces. When a liquid droplet on a rough rigid surface evaporates, suspended particles are deposited along the perimeter. Edge of such an evaporating drop is pinned on the solid surface. After evaporation a ring of highly concentrated particles is formed. This well known phenomenon coffee ring effect is a potentially useful technology impacting printing, washing and coating processes. Using a colloidal suspension of gold particles it might be possible to assemble a fine wire with dimensions comparable to those achieved with modern lithographic methods. It might also be possible to stretch DNA using the strong shear flow that develops in ring forming drops when the evaporation rate is enhanced at the edge.[1] Ring deposits also provide a potential means to write or deposit a fine pattern onto a surface[2]. Modelling such a process involves accounting for mass, momentum and energy trasport in liquid and gas phases. Adding to the complexity of the problem, physical systems involve changes in the surface energy and topography of the solid. The resulting problem is thus challenging from a computational perspective.

The method of lines (MOL) is a technique for solving partial differential equations (PDEs) in which all but one dimension is discretized. The method of lines most often refers to the construction or analysis of numerical methods for partial differential equations that proceeds by first discretizing the spatial derivatives only and leaving the time variable continuous. This leads to a system of ordinary differential equations to which a numerical method for initial value ordinary equations can be applied. The method of lines in this context dates back to at least the early 1960s.

Lattice-Boltzmann (LB) simulations have become a standard tool in computational fluid dynamics. Instead of solving the Navier Stokes equations, the discrete Boltzmann equation is solved to simulate the flow of a Newtonian fluid with collision models such as Bhatnagar Gross Krook (BGK). By simulating streaming and collision processes across a limited number of particles, the intrinsic particle interactions evince a microcosm of viscous flow behavior applicable across the greater mass. LB method is scalable for parallel computing. Recently, LB simulations have proved useful to gain insight in complex geometries. A particular advantage that an LB treatment of evaporation would bring is the possibility of studying evaporation in the presence of flow and on complex microstructured surfaces.

In this study, we validate modeling evaporation and condensation using LB method and method of lines. We simulated evaporation and condensation of planar droplets, evaporation of a sessile droplet on an ideal and non-ideal solid surface.

Governing equations

Continuity equation,

$$\frac{\partial \rho}{\partial t} + \nabla.(\rho \vec{v}) = 0 \tag{1}$$

Navier-Stokes equation,

$$\rho[\vec{v} + (\vec{v}.\nabla)\vec{v}] = \eta \nabla^2 \vec{v} - \phi \nabla \mu - \nabla P \tag{2}$$

Cahn-Hilliard convection-diffusion equation,

$$\frac{\partial \phi}{\partial t} = \nabla.(\phi \vec{v}) + \nabla.(M \nabla \phi) \tag{3}$$

where ϕ is the phase field and M is *mobility parameter* which plays the role of diffusivity.

Lattice-Boltzmann method

Instead of solving equations (1)-(3), the discrete Boltzmann equation is solved to simulate the flow of a Newtonian fluid.

$$f_i(\mathbf{r} + \mathbf{c}_i \Delta t, t + \Delta t) - f_i(\mathbf{r}, t) = -\frac{\Delta t}{\tau}(f_i - f_i^{eq}) \tag{4}$$

$$g_i(\mathbf{r} + \mathbf{c}_i \Delta t, t + \Delta t) - g_i(\mathbf{r}, t) = -\frac{\Delta t}{\tau_g}(g_i - g_i^{eq}) \tag{5}$$

Hydrodynamic variables are related to above velocity distribution functions by,

$$\rho \equiv \sum_i f_i, \quad \rho v_\alpha \equiv \sum_i c_{i\alpha} f_i, \quad \phi \equiv \sum_i g_i \tag{6}$$

Also,

$$\sum_i f_i^{eq} \equiv \rho, \quad \sum_i c_{i\alpha} f_i^{eq} \equiv \rho v_\alpha, \quad \sum_i g_i^{eq} \equiv \phi \tag{7}$$

Expressions for equilibrium distribution functions are reported in [3].

LB Method and Method of Lines

Equation (3) can be solved using method of lines. In this section, we compare various aspects of algorithms of LB method(LBM) and method of lines(MOL)

Time complexity

Average time required for one iteration in both the algorithms was noted and plotted in Figure 1a. It was noted that time for one iteration of MOL is almost equal to LB method with D2Q9 lattice. Time varies linearly with number of points for both the algorithms. Hence both shows time complexity of $\mathcal{O}(n)$

Space complexity

Both the algorithms have same space complexity $\mathcal{O}(n)$

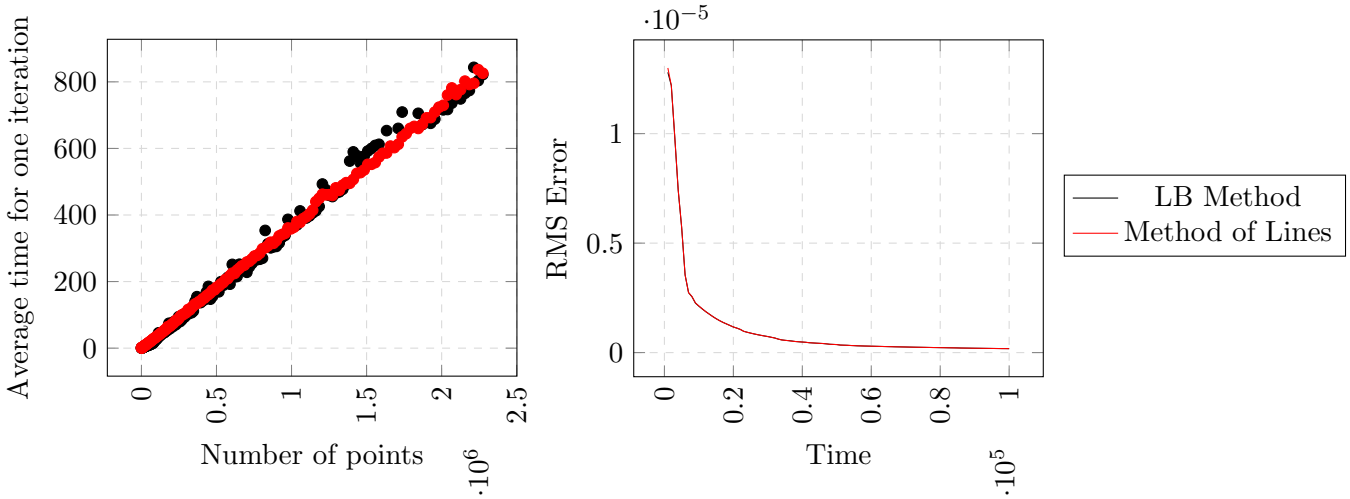

(a) Average time for one iteration vary linearly for both the methods

(b) Both the algorithms show same time for convergence

Figure 1: Time complexity and convergence analysis for LB method and method of lines

Time for convergence

It was noted that both the methods gives almost same result and error at a particular time and takes almost same time to converge to a solution.

Spinodal decomposition

Spinodal decomposition is a mechanism for the rapid unmixing of a mixture of liquids or solids from one thermodynamic phase, to form two coexisting phases. Refer Figure 2 for the spinodal decomposition simulation where we started with each point having a random ϕ value where $-1 \leq \phi \leq 1$.

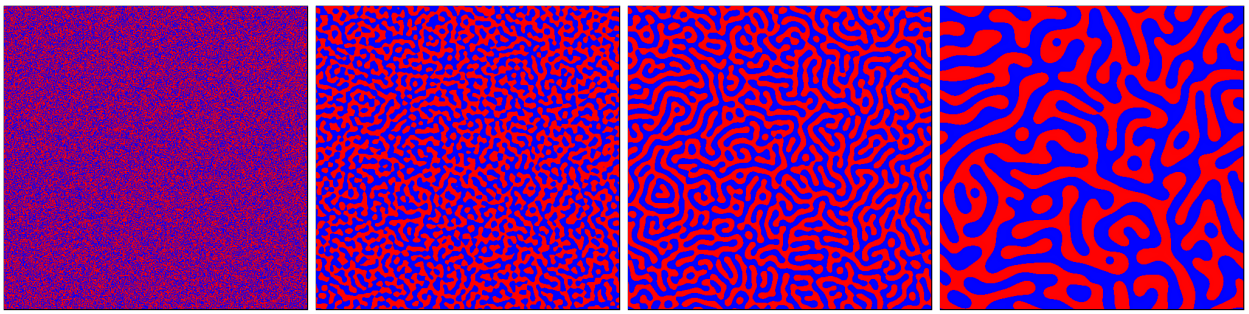

(a) t = 0 (b) t = 1000 (c) t = 10000 (d) t = 100000

Figure 2: Spinodal decomposition simulation in a domain of 500 * 500 using Lattice Boltzmann method. It can be seen that phases unmix to form separate clusters.

[Click here to see the video of the simulation.]

Surface tension

Surface tension is the elastic tendency of a fluid surface which makes it acquire the least surface area possible. For any volume, sphere gives the least surface area. In the following simulation, a cubic volume of liquid is taken at t = 0. As expected, the droplets changes itself to a spherical droplet. (Refer Figure 3)

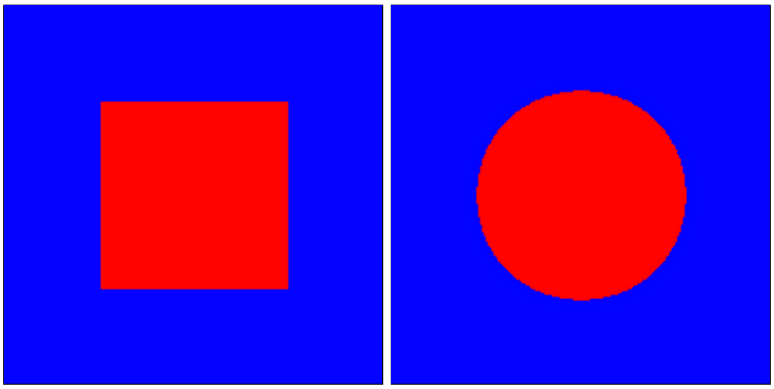

(a) At t = 0 (b) At equilibrium

Figure 3: Evolution of a square surface to a circular surface.

Variation of phase field close to interface

Close to interface, the phase field varies as a hyperbolic tangent with the normal coordinates to the interface, r. Simulation data was perfectly matching with the numerical solution given by [4]. (Refer Fig 4)

$$\phi(r) = \phi_{eq} tanh(\frac{r}{\epsilon}) \tag{8}$$

where $\phi_{eq} = \sqrt{-a/b}$ and $\epsilon \equiv \sqrt{-2k/a}$ is the interface thickness

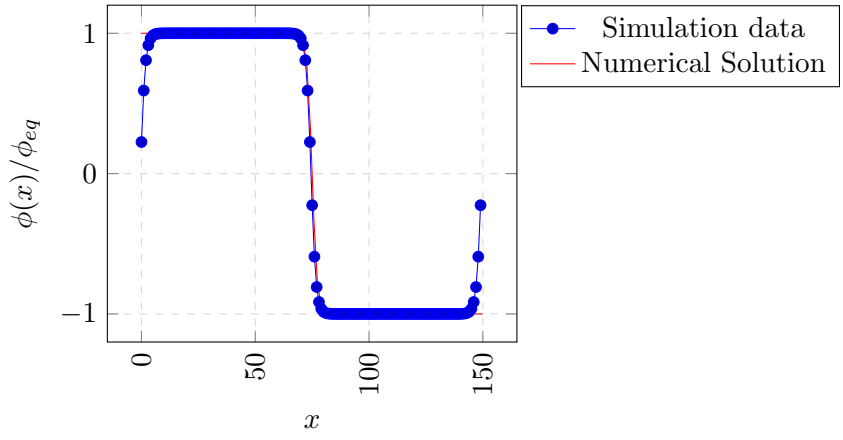

Figure 4: Phase field profile along normal to interface of two already separated phases

Solid wall

Bounce-back rules [5] are imposed along the boundary for impenetrability and no-slip boundary conditions. Also,

$$\vec{n}.\nabla\mu = 0 \tag{9}$$

For an equilibrium contact angle on an ideal solid wall, geometrical formulation is used for implementing wetting condition [6, 7].

$$\phi_{i,j,1} = \phi_{i,j,3} + tanh(\frac{\pi}{2} - \theta)\xi \tag{10}$$

where

$$\xi = \sqrt{(\phi_{i+1,j,2} - \phi_{i-1,j,2})^2 + (\phi_{i,j+1,2} - \phi_{i,j-1,2})^2} \tag{11}$$

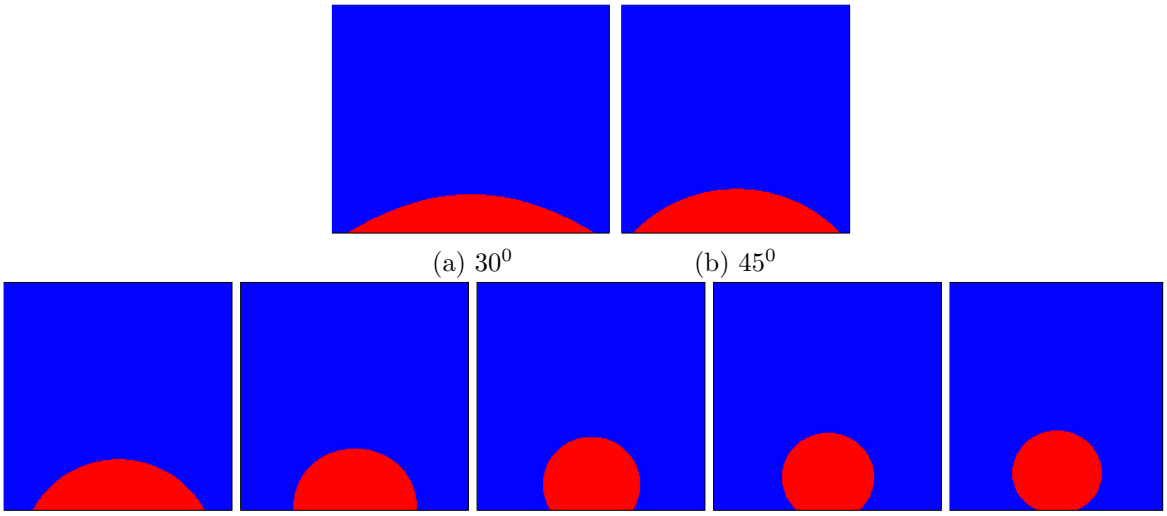

(a) 30^0 (b) 45^0 (c) 60^0 (d) 90^0 (e) 120^0 (f) 135^0 (g) 150^0

Figure 5: Droplets on solid wall with different contact angles

Evaporation of a planar droplet

To drive evaporation of the film we impose the boundary condition $\phi(z = z_H, t) = \phi_H$, where $\phi_H < -\phi_{eq}$. This induces a gradient in the chemical potential field μ. In response to this imbalance, the system reduces ϕ, which corresponds to the evaporation of the film[8]. Phase field imbalance, $\Delta\phi_H \equiv -\phi_{eq} - \phi_H$

We performed simulations in a box consisting of 1 x 1 x 150 lattice sites. Periodic boundary conditions were set in the x and y directions. A wall was located at $z_w = 1$, while the concentration was fixed to a value ϕ_H at $z_H = N_z$ to drive the system out of equilibrium. The initial height of the film was set to $z_0 = 100$. Figure 6a shows that height of droplet decreases faster as driving force $\Delta\phi_H$ increases. Figure 6b shows height of the drop decreasing with time.

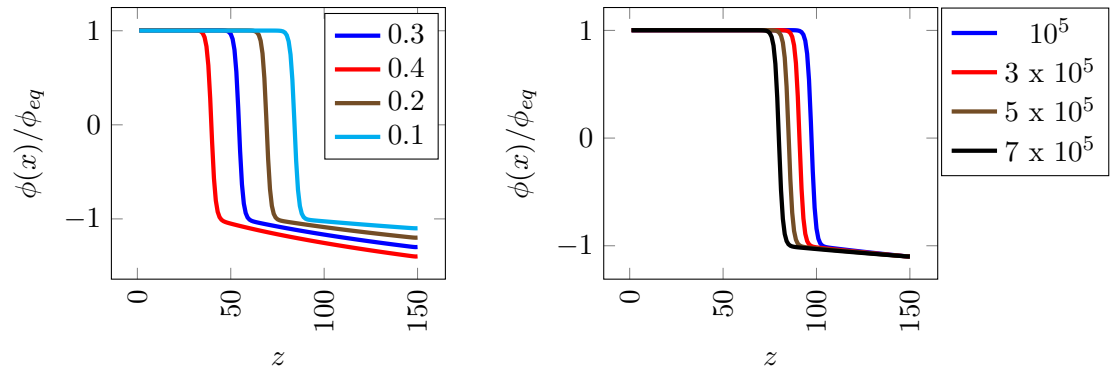

(a) After 5 x 10^6 simulation steps with different ϕ_H

(b) Phase field profile at different time steps

Figure 6: Phase field profile for the planar film evaporation.

Condensation of planar droplet

Similar to evaporation, condensation can be simulated by imposing boundary condition $\phi(z = z_H, t) = \phi_H$, where $\phi_H > -\phi_{eq}$. In Figure 7, a planar droplet of height 100 is evaporated with

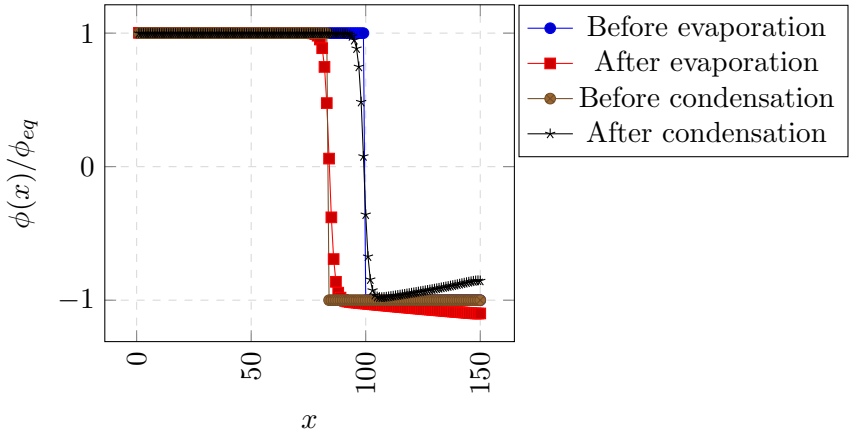

Figure 7: Phase field profile along normal to interface of evaporating and condensing planar droplet.

$\phi_H = -1.1$. After 5 x 10^6 timesteps, boundary condition at z = 150 is changed to $\phi_H = -0.85$ (at which μ is equal and opposite to that of $\mu(\phi = -1.1)$) to initiate evaporation. It is observed that after condensing for same duration as that of evaporation, at t = 10 x 10^6 the system returns to the initial condition.

Evaporation and condensation of a sessile droplet on a solid surface

12.1 Ideal surface

An ideal solid surface is flat, rigid, perfectly smooth, and chemically homogeneous, and has zero contact angle hysteresis. On such a surface, only one thermodynamically stable contact angle exists. Hence we expect a constant contact angle and varying contact diameter during evaporation and condensation.

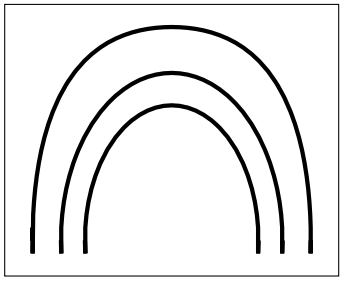

Figure 8: Shape profile of an evaporating droplet on an ideal surface.

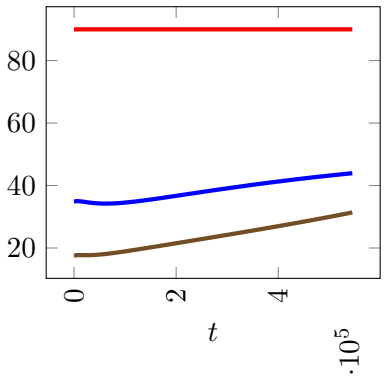

(a) Condensation

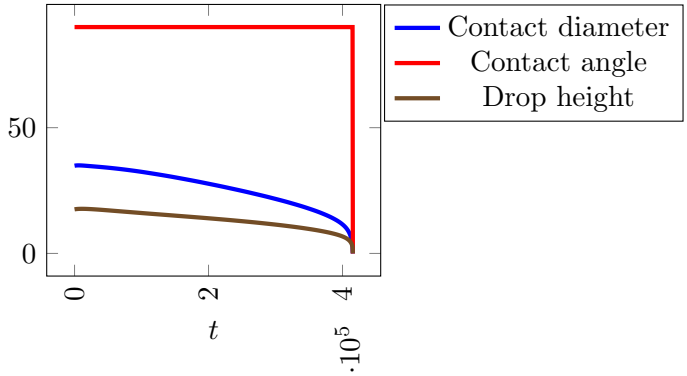

(b) Evaporation

Figure 9: Contact diameter, angle and drop height of a droplet on an ideal surface with equilibrium contact angle 90^0 during evaporation/condensation.

12.2 Hysteretic surface

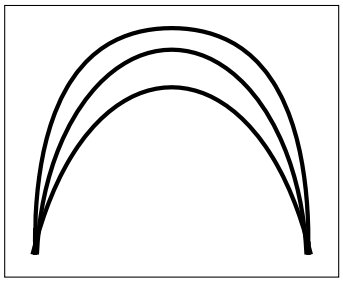

Figure 10: Shape profile of an evaporating droplet on a hysteretic surface.

In many natural systems, the solid walls are usually rough and chemically inhomogeneous. In these surfaces, contact angle hysteresis has to be taken into consideration. Due to hysteresis, the contact line remains pinned when the local contact angle θ is within a hysteresis window.

$$\theta_R \leq \theta \leq \theta_A \tag{12}$$

where θ_R and θ_A denote the receding angle and advancing angle respectively.
When θ is greater than θ_A, the contact line moves forward. When θ is less than θ_R, the contact line moves backward. To realize this effect, at each time step of computation, we should first obtain the local apparent contact angle at the contact points. Then, comparisons of θ with θ_R and θ_A are required. If $\theta \leq \theta_R$, θ in Eq.11 should be replaced by θ_R; if $\theta \geq \theta_A$, θ should be replaced by θ_A; else θ in Eq.11 remains unchanged.

A small difference in contact angle imposed using Eq.11 and measured contact angle was observed in the simulation. This difference was causing error while implementing contact angle hysteresis, i.e, the contact angle θ was reaching θ_R at a very short time causing contact angle pinning to be visible for very small duration. Hence, difference between measured angle and imposed angle was plotted in Figure 11 and this data was used to correct the measured angle.

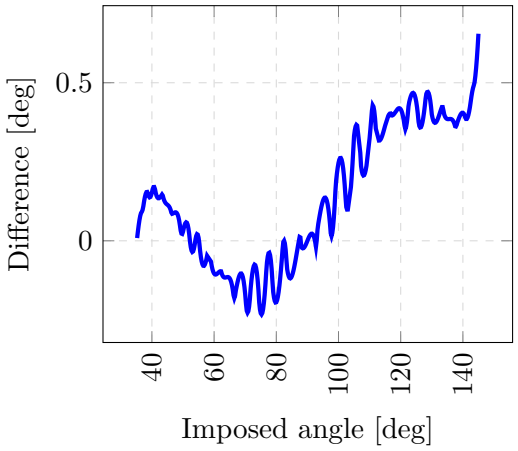

Figure 11: Difference between imposed contact angle and measured contact angle

Picknett and Bexon[9] followed the mass and profile evolution of organic liquid drops. They observed three distinct evaporation modes: mode 1, during which the solid and iquid interface area

remains constant (when hysteresis exists); mode 2, for which the contact angle remains constant (ideal system with no hysteresis at equilibrium); mode 3, which is a mixed mode. They also observed that evaporation follows the first mode until $\theta = \theta_R$, and then, the second mode is initiated.[10]

In Figure 12 a droplet with initial contact angle 90^0 is evaporating on a surface with $\theta_R = 42^0$ and $\theta_A = 140^0$. It followes mode 1 in the initial stage where contact diameter stays constant whereas contact angle decreases. After contact angle reaches $\theta = \theta_R$, mode 2 is observed in which contact angle stays at θ_R and the contact diameter reduces.

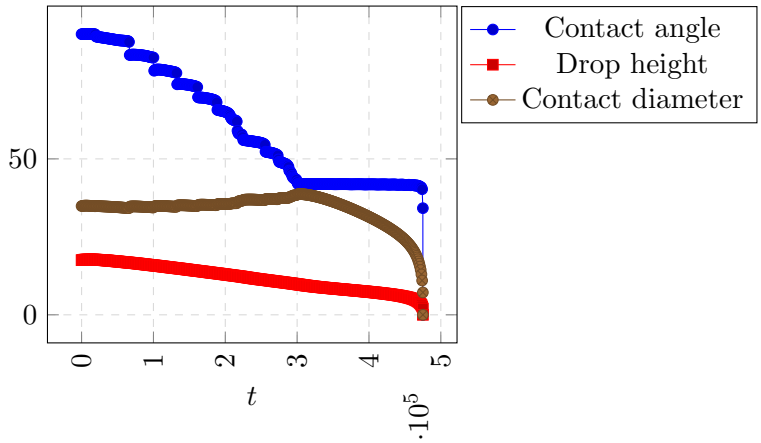

Figure 12: Profile of a evaporating droplet on a hysteretic surface.

In Figure 13 a droplet with initial contact angle 70^0 is condensing on a surface with $\theta_R = 42^0$ and $\theta_A = 90^0$. In the early stage, contact line is pinned (constant contact diameter) as the contact angle increases to θ_A. Once the θ reaches θ_R contact angle stays at θ_A and contact diameter also increases with drop height.

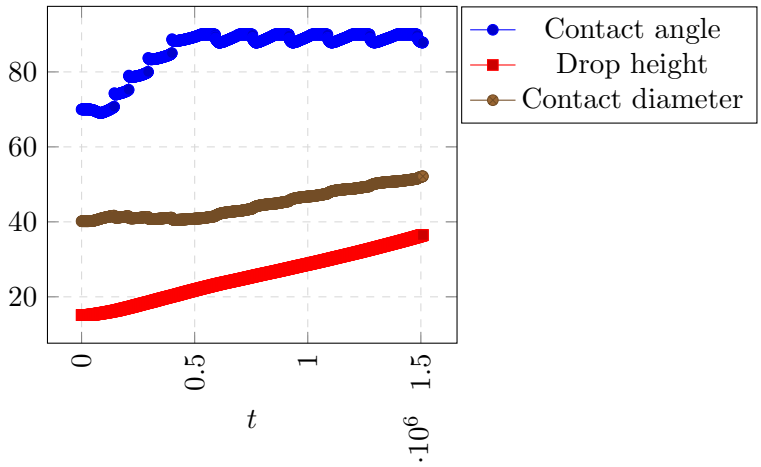

Figure 13: Profile of a condensing droplet on a hysteretic surface.

Discussion and Conclusions

We discussed two methods for study of evaporation and condensation - Lattice Boltzmann algorithm and Method of lines. Both of the methods show $\mathcal{O}(n)$ time complexity and $\mathcal{O}(n)$ space complexity. Time for one iteration of 4th order Runge Kutta method and LB method on D2Q9 lattice was found to be almost same. Both the methods showed identical error from previous time steps and time for convergence. Both methods were validated by simulating spidodal decomposition, evolution of a square surface into a circular one and studying variation of phase field close to interface.

Evaporation was implemented by imposing a boundary condition $\phi(z = z_H, t) = \phi_H$, where $\phi_H < -\phi_{eq}$. This induces a gradient in the chemical potential field μ. In response to this imbalance, the system reduces ϕ, which corresponds to the evaporation of the film[8]. A reverse effect was observed when boundary condition $\phi(z = z_H, t) = \phi_H$, where $0 > \phi_H > -\phi_{eq}$. Hence we were able to simulate condensation in the system. With equal chemical potential gradient, amount of liquid evaporated was found to be equal to that of condensated (Refer Figure 7).

Wetting condition proposed by H. Ding and P. D. M. Spelt[7] was found to have a difference between imposed and measured angle. It can reduce time in hysteresis window drastically. For correct study of contact angle hysterisis, this should be corrected by mapping measured contact angle to difference between imposed and measured angle. This difference should be added to measured angle as a correction.

Evaporation and condensation was studied on a ideal and non-ideal surface. On an ideal surface during the both process, contact angle stays constant whereas contact diameter and drop height changes. On a hysteretic surface, contact dimater was staying constant until contact angle reaches θ_R or θ_A after which contact angle was staying constant. This result was in accordance with experimental results recorded by Picknett and Bexon[9]. Contact line was pinned when θ is in the hysteresis window. A complete pinning of the contact line can be achieved by imposing $\theta_R = 0^0$ or $\theta_A = 180^0$

Future work

In this study, we were able to implement contact line pinning along with evaporation. Flow of fluid and particles can be incorporated in this model to study coffee ring effect. While simulating evaporation, a constant driving force was applied on the system. However, in real world this may not be the case. A varrying driving force could more accurately model the process.

Source code

The entire simulation was done using Java8. Source code is shared on a public repository in GitHub. Link - https://github.com/aqelkp/Coffee-ring-effect

References

[1] C. M. R. Center, "Why do drying drops leave a ring stain?."

[2] R. Deegan, O. Bakajin, T. Dupont, G. Huber, S. Nagel, and T. Witten, "Capillary flow as the cause of ring stains from dried liquid drops," *Nature*, vol. 389, no. 6653, pp. 827–829, 1997.

[3] J.-C. D. I. P. P. B. V. M. Kendon, M. E. Cates, "Inertial effects in three dimensional spinodal decomposition of a symmetric binary fluid mixture: A lattice boltzmann study," *J. Fluid Mech. 440 (2001) 147-203*, 2000.

[4] I. P. P.T. Sumesh and R. Adhikari, "Lattice boltzmann - langevin simulations of binary mixtures," *Phys. Rev. E 84, 046709 (2011)*, 2011.

[5] A. J. C. L. Verberg, "Lattice-boltzmann simulations of particle-fluid suspensions," *Journal of Statistical Physics*, vol. 104, no. 5, pp. 1191–1251, 2001.

[6] H.-b. H. Lei Wang and X.-Y. Lu, "Scheme for contact angle and its hysteresis in a multiphase lattice boltzmann method," *Phys. Rev. E 87, 013301*, 2013.

[7] H. Ding and P. D. M. Spelt, "Wetting condition in diffuse interface simulations of contact line motion," *Phys. Rev. E*, vol. 75, p. 046708, Apr 2007.

[8] R. Ledesma-Aguilar, D. Vella, and J. M. Yeomans, "Lattice-boltzmann simulations of droplet evaporation.," *Soft Matter*, vol. 10, no. 41, pp. 8267–8275, 2014.

[9] R. Picknett and R. Bexon, "The evaporation of sessile or pendant drops in still air," *Journal of Colloid and Interface Science*, vol. 61, no. 2, pp. 336 – 350, 1977.

[10] C. Bourges-Monnier and M. E. R. Shanahan, "Influence of evaporation on contact angle," *Langmuir*, vol. 11, no. 7, pp. 2820–2829, 1995.